Acta Materialia 226 (2022) 117622

Contents lists available at ScienceDirect

Acta Materialia

journal homepage: www.elsevier.com/locate/actamat

Hydrogen induced dislocation core reconstruction in bcc tungsten

Yu-Hao Li[a,b], Hong-Bo Zhou[a,b,*], Fei Gao[c], Gang Lu[d], Guang-Hong Lu[a,b,*], Feng Liu[e,**]

[a] Department of Physics, Beihang University, No. 37, Xueyuan Road, Haidian Distr, Beijing 100191, China
[b] Beijing Key Laboratory of Advanced Nuclear Materials and Physics, Beihang University, Beijing 100191, China
[c] Department of Nuclear Engineering and Radiological Science, University of Michigan, Ann Arbor, MI 48109, USA
[d] Department of Physics and Astronomy, California State University Northridge, Northridge, CA 91330-8268, USA
[e] Department of Materials Science and Engineering, University of Utah, UT 84112, USA

ARTICLE INFO

Article history:
Received 31 August 2021
Revised 3 January 2022
Accepted 3 January 2022
Available online 5 January 2022

Keywords:
Screw dislocation
Core structure
Dislocation motion
Hydrogen and interstitial solutes
Bcc tungsten

ABSTRACT

Dislocation, playing a crucial role in the plastic deformation of metals, can be significantly affected by introducing solute elements. Hydrogen (H) embrittlement is one such example, while the underlying mechanism for H affected dislocation structural stability and mobility remains unclear and the role of H has been controversial. Here, using first-principles calculations, we demonstrate that the effect of H on screw dislocation in bcc tungsten (W) is H concentration-dependent, signified by a H-induced transition of SD core structure. At low concentrations of H segregation, dislocation maintains the intrinsic easy-core structure, and H atoms are attached to the "periphery" of dislocation to enhance dislocation motion. In contrast, at high H concentrations, dislocation transforms into a hard-core, metal hydride-like structure, as H atoms become the "body" of dislocation to significantly reduce the dislocation mobility in W. Further, such local easy-to-hard transition can also be induced by the other solutes, including helium, carbon, nitrogen and oxygen. Our work sheds new light on the H-dislocation interactions in bcc W, having broad implications in the interstitial solute-related phenomena.

© 2022 Acta Materialia Inc. Published by Elsevier Ltd. All rights reserved.

1. Introduction

As primary carrier of plastic deformation, dislocation plays a dominant role in affecting many properties of crystalline materials [1–4]. The presence of solute elements, either naturally existing or intentionally added, can interact strongly with the dislocation and drastically alter its properties such as mobility [5–7]. One prominent example is hydrogen embrittlement (HE), which is one of the most important problems in materials science and engineering because almost all metals and their alloys suffer to some extent from the H-induced brittleness [8–11]. Despite decades of enormous research effort, there is no consensus on HE mechanisms and controversies abound in literatures [12–18]. Among the proposed mechanisms, the H-dislocation interaction is considered critically important, because it plays a key role in determining the mechanical properties of materials, such as facture formation and crack growth [17–20]. Therefore, fundamental understanding of the nature of H-dislocation interaction, especially the effect of H on dislocation structural stability and mobility, is of crucial importance.

Like other solutes [21–23], H is known to segregate into dislocations to relieve local stress [24]. However, how H segregation will affect the dislocation structure, stability and hence mobility remains a very challenging and highly controversial problem. For example, two opposite influences of H on dislocation mobility have been proposed. On the one hand, Cottrell put forward an early theory which suggests mobile foreign atoms segregate into to the dislocation to form a Cottrell atmosphere surrounding the dislocation core [25], to inhibit dislocation motion. It has been supported by some experiments [20] and atomistic simulations [17,26,27]. On the other hand, other experiments have demonstrated that introduction of H may reduce the flow stress and increase the velocity of dislocations in metals [28–31]. The H-enhanced dislocation motion was rationalized by H-shielding of elastic interaction between dislocations and H-modified atomic bonding in the dislocation core [19,32,33]. Making the matter even more complicated, both pinning and enhancing effects of H on dislocation mobility have been suggested based on first-principles calculation employing semi-empirical models [34,35], which simply considers the interaction between only one H and the screw dislocation (SD) core. Since the binding energy of H with hard-core structure (approximated as the saddle point of SD movement) is higher than that of

* Corresponding authors at: Department of Physics, Beihang University, No. 37, Xueyuan Road, Haidian Distr, Beijing 100191, China.
** Corresponding author at: Department of Materials Science and Engineering, University of Utah, UT 84112, USA.
E-mail addresses: hbzhou@buaa.edu.cn (H.-B. Zhou), lgh@buaa.edu.cn (G.-H. Lu), fliu@eng.utah.edu (F. Liu).

https://doi.org/10.1016/j.actamat.2022.117622
1359-6454/© 2022 Acta Materialia Inc. Published by Elsevier Ltd. All rights reserved.

easy-core configuration (i.e., ground state), the H segregation reduces the energy barrier of dislocation motion but the SD remains the easy-core structure [34]. More recently, using the segregation energies of a single H in the vicinity of SD as input, a kinetic Monte Carlo simulation proposed an easy-to-hard core transformation induced by H segregation in bcc Fe, which is associated with SD mobility and identified as "30 appm anomaly" [36]. In that work, H segregation was shown to always increase dislocation velocity, despite hard core formation [36]. However, such single-H induced SD core transformation contradicts with other atomic simulations showing single H segregation to easy-core SD in both Fe and W [22,27,32,34,37].

Here, using SD in bcc W as a prototypical example, we demonstrate that the effects of H are strongly dependent on H concentration, highlighted by a H-induced dislocation core reconstruction beyond single H segregation, based on comprehensive first-principles calculations. Our focus on SD is made since low-temperature microstructure of bcc metals are predominantly controlled by the screw components. At low concentrations of H segregation, less than one H per period, H atoms are effectively attached to the "periphery" of SD, without changing the original intrinsic easy-core structure. The one H can occupy multiple local energy-minimum positions next to the SD core, tending to enhance the dislocation mobility by moving along with SD in a concerted fashion via the local minima. In contrast, at high H concentrations, more than two H within any period, the SD core will transform either locally or globally into a hard-core structure, where H atoms become the "body" of the SD forming a metal hydride-like core, tending to pin dislocation motion in W. Calculations of maximum Peierls stress, which about tripled in the H-rich hard-core configurations, confirm the expectation on dislocation mobility. Furthermore, the segregation of most other solutes, such as He, C, N and O, will induce a local easy-to-hard transition and appear to pin the SD motion in W.

2. Computational method

2.1. First-principles calculations

Based on the density functional theory (DFT), our first-principles calculations were performed using the VASP code [38,39] with the projector augmented wave (PAW) method [40]. The exchange-correlation functional is described by the Perdew-Burke-Ernzerhof (PBE) form within generalized gradient approximation (GGA) [41]. 5*d*/6 s electrons for W, 1 s for H/He and 2 s/2*p* for C/N/O were included as valence electrons. In all calculations, the atomic positions and lattice parameters were fully relaxed according to the Hellmann-Feynman force (less than 0.01 eV/Å for all atoms), and the kinetic-energy cutoff for plane wave functions was set to 400 eV.

A 128-atoms supercell ($4a_0 \times 4a_0 \times 4a_0$) was employed to model interstitial solutes in bulk W, with the *k*-point grid of $3 \times 3 \times 3$ in the Monkhorst-Pack scheme [42]. To model the 1/2<111> screw dislocation, we employ the periodic dislocation dipole approach, with two dislocations of antiparallel burgers vector ($\vec{b}$) included in the super cell (135-atoms per burgers vector). Generally, there are two different dislocation arrangements in the dipole approach [43,44]. The first one is a triangular periodic array of dislocation dipoles, which leads to the three-fold symmetry of the crystal in the ⟨111⟩ direction. The second arrangement is equivalent to a square-like periodic array of quadrupoles. As discussed previously [43,44], the quadrupole arrangement, which we used, converges the dislocation core energy faster than the triangular array. To simulate the interstitial solutes, the supercell was extended along the dislocation line, using 270- (2*b*) and 405-atom (3*b*) supercells for treating the number of H atoms (n) in the SD with $n < 3$ and $n \geq 3$, respectively. The Brillouin zone was correspondingly sampled with $1 \times 2 \times 16$, $1 \times 2 \times 8$ and $1 \times 2 \times 6$ *k*-points grids for the supercells of 1*b*, 2*b* and 3*b* length along the core, respectively. The interstitial solutes are introduced at both SDs to extract energy per SD. Furthermore, the climbing image-nudged elastic band (CI-NEB) method [45,46] with five intermediate replica images was employed to determine the H diffusion barriers and Peierls barriers of SD in W. For the SD motion, two dislocations move into adjacent stable sites simultaneously and their distance remains constant.

2.2. Calculation of Peierls stress

Similar to previous studies [47,48], the Peierls stress of SD was calculated in a strained supercell, in which the cell vectors were modified gradually until the dislocations start to move as $\vec{C}_{2,\varepsilon} = \vec{C}_2 + \varepsilon\vec{u}_{[111]}$. $\vec{C}_{2,\varepsilon}$ and $\vec{C}_2$ are the cell vectors before and after, respectively. ε is the applied strain and $\vec{u}_{[111]}$ is the basis vectors connecting two atoms along the [111] direction. The strain-induced stress (σ_{yz}) exerts a Peach-Köhler force on the dislocation, driving it to move along the [112] direction. Usually, the applied strain (ε_{yz}) induces not only stress components σ_{yz} but also σ_{xy}, but the latter was verified to be negligible in our cases with $\sigma_{xy}/\sigma_{yz} < 0.08$. To ensure the accuracy of this calculation, we use a very small step size in ε, to generate a stress variation of $\sim$ 0.01 GPa close to the Peierls stress.

Since the periodic dislocation dipole approach was employed, the Peierls stress obtained from DFT calculations differs somewhat from that of the isolated dislocation and should be corrected by considering the elastic interaction between dislocations. Employing a supercell with a dislocation dipole, the energy increase (ΔE) relative to bulk has two parts, the linear-elastic interaction energy between dislocations (E_{el}) and the dislocation core energy (E_{core}), i.e. $\Delta E = E_{el} + 2E_{core}$. Hence, the Peierls stress is obtained directly from DFT calculations as $\sigma_P^{DFT} = \frac{1}{b^2}\frac{\partial \Delta E}{\partial d}|_{d=d^*}$, where d is the dislocation distance and d^* is the distance for the highest derivative, i.e. $d^* = 7d_0$ (d_0 being the distance between two nearest Peierls valleys). Accordingly, the Peierls stress of an isolated dislocations is $\sigma_p = \frac{1}{b^2}\frac{\partial E_{core}}{\partial d}|_{d=d^*}$ and $\sigma_P^c = \frac{1}{b^2}\frac{\partial E_{el}}{\partial d}|_{d=d^*}$ is the correction term that arises from the elastic interaction between dislocations. Thus, the Peierls stress of an isolated dislocation can be calculated by $\sigma_p = \sigma_P^{DFT} - \sigma_P^c$. Here, adopting an approach proposed by Cai et al. [49,50], we calculated the elastic energy, as obtained from a Madelung summation (http://micro.stanford.edu/~caiwei/Forum/2004–08–08-MadSum) using the experimental elastic constants and crystal parameters [51], with the cutoff ratio set at the Burgers vector. Since the concentration of interstitial solutes in W is extremely low ($\sim 10^3$ appm), their effects on the elastic constants and long-range stress field of SD are neglected, so the addition of correction will not change the variation trend of Peierls stress.

2.3. Calculation of kink-pair formation enthalpy

Specifically in the line tension model [52,53], the dislocation is considered as a line defect moving in the Peierls potential $U(u)$, with U being the energy per unit length of a straight SD at a distance u displaced from the equilibrium position and a line tension energy γ_d penalizes the length increment relative to a straight dislocation. Then, the kink-pair enthalpy is calculated by the energy difference between a kinked and a straight dislocation as [54]

$$H_{kp}(\sigma^*) = 2(2\gamma_d)^{1/2}\int_{u=\bar{u}}^{u=u_{max}}[U(u) - U(\bar{u}) - (u-\bar{u})b\sigma^*]^{1/2}du, \quad (1)$$

where b is burgers vector and $\bar{u}$ denotes the saddle point position of a straight dislocation under applied stress σ^*, i.e. $\frac{dU}{du}|_{u=\bar{u}} = b\sigma^*$.

$u_{max}$is defined as

$$U(u_{max}) - U(\bar{u}) = (u_{max} - \bar{u})b\sigma^*. \quad (2)$$

Here, the Peierls stress (σ_P) is the maximum value that the applied stress can attain to move the dislocation without thermal activation, i.e. $\sigma_P = \frac{1}{b}(\frac{dU}{du})_{max}$. Assuming the Peierls potential of W with a sinusoidal shape (which is confirmed by ours and previous DFT calculations [55]), it can be expressed as

$$U(u) = \frac{d_0 b\sigma_P}{2\pi}\left[1 - \cos\left(\frac{2\pi u}{d_0}\right)\right]. \quad (3)$$

Then, the kink-pair enthalpy without external stress ($\sigma^* = 0$) can be obtained as

$$H_{kp}(\sigma = 0) = Zd_0\sqrt{2\gamma_d d_0 b\sigma_p}, \quad (4)$$

where Z is a constant related to the shape of Peierls potential ($Z = 4/\pi^{3/2}$ for a sinusoidal shape). The line tension of an isolated SD can be calculated as $\gamma_d = \frac{Kb^2}{(4\pi)\ln(\frac{R}{r_c})} + E_{core}$, including the elastic energy (R/r_0 the outer/inner cut-off radius of dislocation stress field) and the core energy. The elastic energy can be estimated from the prefactor K, a combination of elastic constants [49], and $\ln(\frac{R}{r_c})$, typically assumed to be $\sim$ 4 [54]. The core energy can be extracted directly from DFT calculations.

Note that this model have been shown to successfully reproduce the kink-pair nucleation enthalpy in pure bcc metals and describe the effects of substitutional alloys with high concentration in a mean-field approximation [48]. This is different from the case in present work, in which the influences of interstitial H with low concentration are determined. Accordingly, there are two prerequisites for the application of this model. The first prerequisite is that the H concentration in the dislocation region is high enough so that a mean-field approach is justified; this point will be discussed in detail in Section 3.3. The second one is that the timescale of H diffusion should be much shorter than that of the migration of SD, thus the H atoms can catch up with the moving SD in W. This is the case in W-H system, because the migration rates of SD are much lower than that of an interstitial H in W, as demonstrated in previous studies [56,57]. Therefore, this model was used in present work to show the influence of interstitial H on the kink-pair formation in W.

3. Results and discussion

3.1. Interaction between SD and a single H atom

Specifically, we investigate atomistic interactions between H and a SD with 1/2<111> Burgers vector, whose structure in bcc W is illustrated in Fig. 1(a). It has a three-fold screw rotation symmetry along the core (chosen as c-axis) [58], $\hat{S} = \{C_3|(\frac{c}{3})\}$. There are three core atoms per period [dark gray spheres in Fig. 1(a)], relatively displaced along the core at (0, c/3, 2c/3) positions. A pair of dislocation dipoles having opposite chirality are used to construct a supercell with periodic boundary condition. Since H atomic radius is only $\sim$ 1/4 of that of W, it energetically prefers to occupy the tetrahedral interstitial site (TIS), as in most bcc metals [59]. Similarly, H is found to also occupy TI-like sites in the vicinity of SD, as shown in Fig. 1(b) [site *A* through *G*, see also Fig. 1(c)]; but with lower energies than in the bulk, as shown in Fig. 1(d). This provides a thermodynamic driving force for H segregating into the SD, similar to other dislocation induced solute segregation. Specifically, H is "attracted" to the SD from $\sim$ 5.5 Å away (*G* site) and then "attached" to the periphery of SD core within 2.26 Å (*A, B, C* sites). The most stable *A, B* and *C* sites have a segregation energy of −0.51 eV, −0.45 eV and −0.50 eV, respectively, as shown in Fig. 1(d). Fig. 1(e) shows the down-hill diffusion path of H from *G* site (close to bulk TIS energy) to *C* site, with an energy barrier of ~0.20 eV in the first step (*G* to *F*), same as in the bulk, and of ~0.24 eV in the rest steps.

It is noted that there are three equivalent *A* sites and six each equivalent *B*/*C* sites. As a H atom is attached to the SD, it may jump in between these stable sites easily with very low barriers, i.e. 72, 128 and 35 meV for *C*→*B*, *B*→*A* and *A*→*A*, respectively, as shown in Fig. 1(f). Interestingly, our simulation results suggest that as the SD moves, H may first relax locally in a concerted fashion with neighboring W atoms, then move along and remain attached to the SD by jumping among these stable sites. For example, Fig. 1(c) illustrates one such case where as the SD moves from left to right (indicated by the curved arrow), one H atom moves first spontaneously from *A* to *C* (dotted straight arrow), and then jumps from *C* to *B* and *B* to *A* (solid straight arrows). This process provides a unique mechanism for H to promote the mobility of SD, by moving concertedly along with all the W atoms involved with the SD motion. This hypothesis is further supported by calculations of the Peierls barriers/stresses.

The Peierls energy barrier of SD in pure W is calculated to be 91 meV/*b*, isotropic along six ⟨112⟩ directions, in a good agreement with previous studies [27,60]. When a H attached to the SD, e.g., at *A* or *B* site, the Peierls barrier becomes anisotropic, as displayed in Fig. 2(a) and (b). Importantly, the largest component of Peierls barrier, indicating the preferred direction of SD motion, is reduced to 57 meV/*b* and 51 meV/*b* for the *A*- and *B*-site H attached SD, respectively, i.e., by 63% and 56% relative to that of SD without H, as shown in Fig. 2(c). This is also verified by examining the generalized stacking fault energy, as the unstable stacking fault energy (γ_{us}) of a 1/2<111>{110} slip system in W is found to decrease with the introduction of a TIS H in the slip plane (see Fig. S1).

To further shed light on the influence of a single H on the dislocation mobility, the atomic configurations of dislocation core for initial state, saddle point and final state of dislocation motion are examined. The case for the initial state with *A*-site H is shown in Fig. 2(d). Initially, the four H-W bonds are almost equivalent with a bond length of 1.85~1.89 Å. At the saddle-point, W atoms are shifted along the [111] direction, while H still resides at the center of a distorted tetrahedron. The H-W bond length increases only slightly to 1.90~2.00 Å, relative to the initial state. At the final state, the SD core moves to the neighboring position resuming the original symmetric core structure, while simultaneously H position is "changed" to the *C* site relative to the new SD position, which is at the center of a pyramid. It is important to realize that the movement of SD is achieved by concerted motion of multiple W atoms in and around SD core predominantly along the c-axis, as indicated by the purple arrows in the lower panels of Fig. 2(d). The presence of H promotes such SD movement by moving along with these W atoms, in a converted fashion relaxing locally, so that there will be relatively smaller increase of W-H bonding energies (see small changes of W-H bond lengths mentioned above) from the initial state to the saddle point, resulting in a reduced Peierls barrier. Similar process is observed for the initial state with *B*-site H, as shown in Fig. 2(e), where upon the SD movement the H "changes" to a different *B* site. In this case, H resides at the center of a tetrahedron at both the initial and final states (four H-W bonds $\sim$ 1.95 Å) and of a prism at the saddle point (six H-W bonds $\sim$ 2.12 Å), respectively.

3.2. Segregation of multiple H atoms into the SD core

So far, we have considered one single H segregated to the SD, where the SD maintains noticeably the original easy-core structure with the H attached. However, our simulations demonstrated that this physical picture is applicable only when less than one H per period is present along the SD core, which can be defined as the upper limit of low concentration for H segregation. Strikingly, a to-

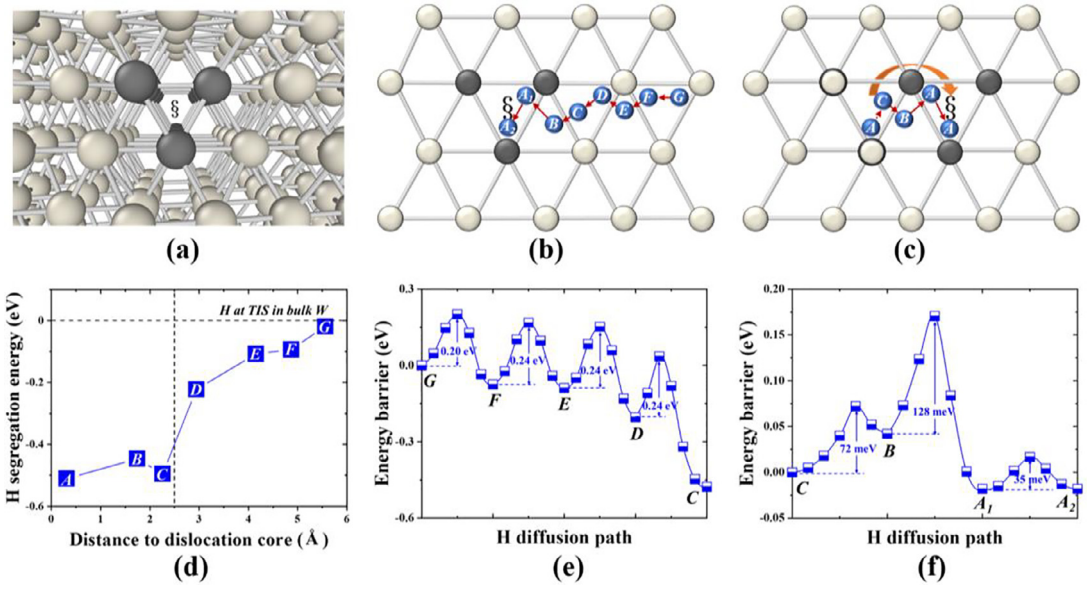

Fig. 1. Segregation of a single H atom from bulk to a 1/2<111> SD in W. (a) Perspective view of the 1/2[111] SD with the easy-core structure in W along the [111] direction chosen as c-axis (out of the page). To create a SD, atomic rows are shifted along [111] direction, creating a chiral structure of choice, as denoted by § sign. (b) One optimal migration pathway for a H (small blue spheres) segregating into the SD core (dark gray spheres), from *G* to *A* site. (c) Concerted motion of one H within one period accompanying the movement of SD. The core atoms before SD motion is represented by milk white balls with black frame. Note that the dashed red arrow indicates a spontaneous (barrier-less) relaxation process of H upon SD motion. (d) H segregation energy as a function of the distance between H and SD core. (e) and (f) Energy barriers at every step of H segregating from site *G* to *C* and from site *C* to *A*, respectively.

tally different story happens at high H concentrations. Whenever there are two H present within any given period, at least the core structure within this period will locally transform into a different hard-core configuration, and at high enough H concentration the whole SD globally transforms into the hard-core configuration. For example, using a large supercell containing a core length of three periods, the first and second H will prefer to occupy among nine possible *A* sites and diffuse along the core almost "freely" with a very low barrier of ∼35 meV as shown in Fig. 1(f), while the SD remains the easy core structure. However, when a third H is added, the *A*-site occupation becomes metastable; instead, it prefers to occupy *B* or *C* site along with another *A*-site H within the same period, and consequently, the local core structure within two periods tend to reconstruct into the hard-core structure [see Figs. S2(a–c) and S3(a–c)]. Adding one more (4th) H, a complete hard-core structure with three H within the same period will be formed [see Figs. S2(d) and S3(d)]. In general, the SD core is infinite long, one may expect that initially at low concentrations, H predominantly occupy and diffuse easily among *A* sites, while maintain the easy-core structure. With increasing H concentration, the hard-core structure starts to emerge locally first with two or three H within a period, and finally with high enough H concentration, the whole SD core becomes hard-core configured with three H per period. Roughly, the transition likely occurs at a H concentration less than one H per period, as illustrated in Fig. 3(c); however, the determination of the exact transition point requires the simulation of an "infinitely" long core with statistical average, which is beyond the scope of the current work.

We note that with three H per period, the hard-core structure looks locally like a monohydride phase with three core W atoms bonded with three H, as shown in Figs. 3(a,b) and S2(e,f). Interestingly, local formation of nano-hydride phase around edge dislocation has also been reported in fcc Ni in a multiscale simulation [61], which is attributed to the H–H attraction and dislocation core relaxation. Here, the H segregation energy per H in the easy-core SD is found to decrease with the increasing H concentration, indicating a repulsive H–H interaction associated with the easy core, similar to their behavior in other defects like vacancies [62], dislocations [63], surfaces [64] and grain boundaries [65]. It indicates that if the SD had kept the easy-core structure, continued H segregation would be prohibited with the increasing H concentration. Interestingly, this scenario is avoided by the H-induced easy-to-hard core transition, as discussed below.

In the hard-core configuration, the second and third H occupy *B*/*C*-type sites, to form a monohydride-like phase with strong and highly symmetric W-H bonds [Fig. 3(a) and (b)]. Surprisingly, as soon as one such local hard-core structure is formed, it may grow rapidly with newly arrived H in a cascade fashion because the subsequently arrived H has a lower segregation energy than the previous one, indicating effectively attractive interaction between H associated with the hard core. For example, the segregation energy of the fifth H is −0.65 eV calculated in a three-period core, notably lower than that of the first H (−0.51 eV). This indicates that the formation of hard-core structure induces an unusual H self-trapping mechanism, in sharp contrast to the H behavior in the easy-core structure and other defects [62–65].

The H-induced transition of SD core structure may be understood via the concept of defactant [66–68], by regarding the hard-core SD as a special "defect" in the easy-core dislocation. In pure W, the formation energy of the "hard-core" defect in the easy core SD is positive. However, with H segregation it becomes negative, leading to a spontaneous easy-to-hard transition. This can be attributed to the strong attraction between H and hard-core. Our calculations show that H segregation significantly lowers the hard-core formation energy by ∼80 mV with one single H per period and makes it be negative with two H per period, providing a thermodynamic driving force for the easy-to-hard core transition (the interactions between a single H and hard-core SD are given in the Supplementary Materials).

Note that the structure of hard core is significantly different from that of easy core. In the easy core, W atoms form a trigonal helix with H atoms located at the center of a tetrahedron (see

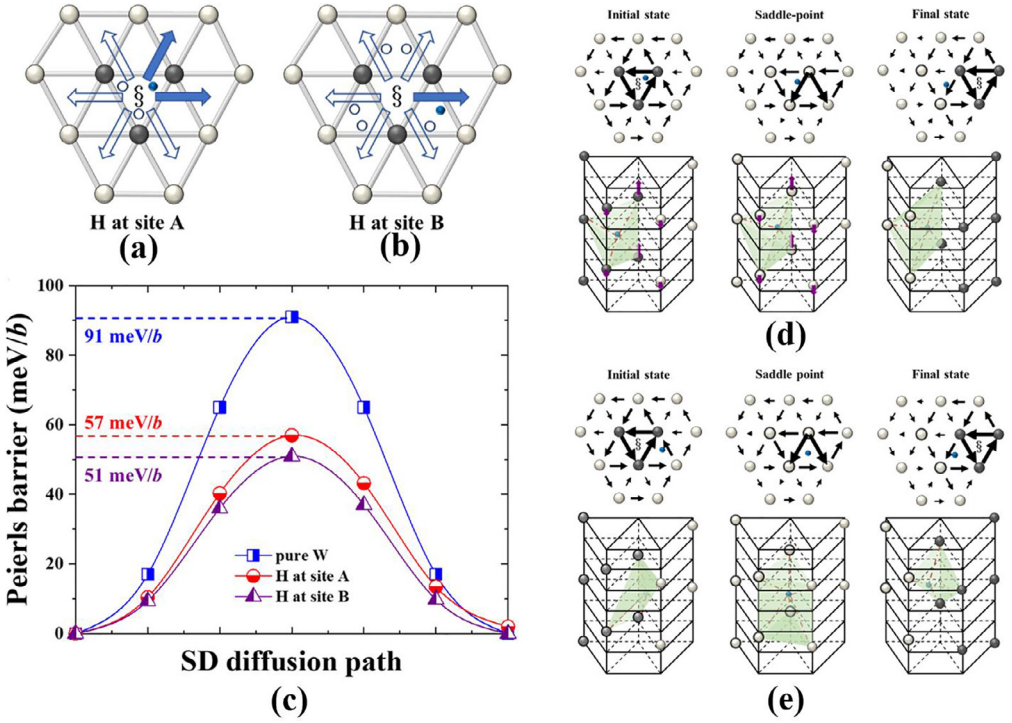

Fig. 2. Visualization of SD motion with a single H atom (blue sphere) with one H attached at (a) *A* site and (b) *B* site initially. Solid blue arrows represent the potential migration direction of the SD, and open blue circles and arrows denote the equivalent H positions and SD migration directions, respectively. (c) The Peierls barrier of SD motion with and without H. The atomic structures illustrating the relative H and neighboring W atom positions at the initial state, saddle point and final state of dislocation motion are shown in (d) and (e) with initial *A* and *B* site H, respectively. Gray and white spheres represent core and other W atoms, respectively. The dash red lines in (d) and (e) show the H-W bonds, and the purple arrows show the direction of W displacements along the [111] direction during the dislocation motion.

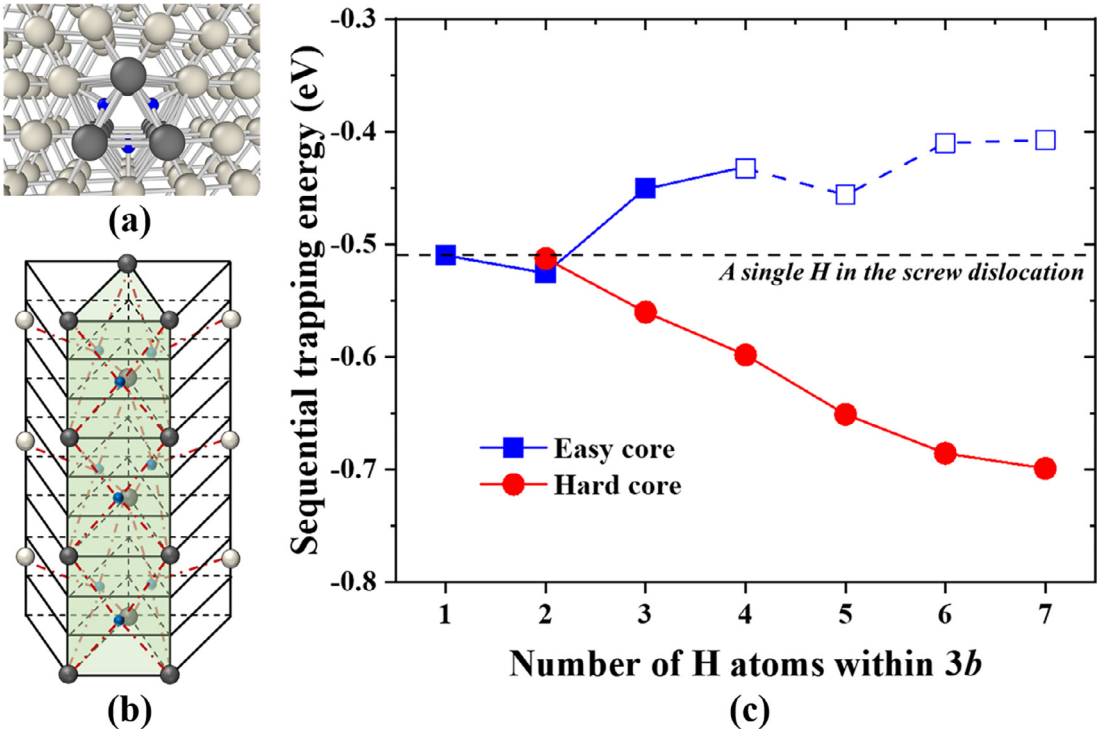

Fig. 3. Schematic illustration of a locally formed hard-core structure, i.e., W_3H_3 hydride-like phase, (a) perspective view and (b) side view. (c) The incremental segregation energy for every additional H in the H_n-SD core. Note that when there are more than three H atoms, the easy-core structure (open blue square) is metastable and easily transfers to the hard-core structure. The segregations of multiple H atoms into the SD core in bcc Mo and Cr are provided in the Supplementary Materials.

Table 1
Interaction of interstitial solutes with the SD in W and its influences on the dislocation core structure and the corrected Peierls stress. Easy and hard core configurations are denoted as *Ec* and *Hc*, respectively. The ratio of Peierls stress (σ^P_{int}) with interstitial solutes to that in pure W (σ^P_{bulk}) is also provided. The system of *SD+3H per period* corresponds the infinite dislocation line that every period looks like a monohydride phase with three core W atoms bonded with three H, as displayed in Fig. 3a and b.

System	Trapping energy	Core structure	Peierls stress	$\sigma^P_{int}/\sigma^P_{bulk}$
Pure SD	/	*Ec*	2.78	1
SD+1H	−0.51	*Ec*	1.59	0.57
SD+2H	−1.03/−1.02	*Ec/Hc*	1.12/3.17	0.40/1.14
SD+3H	−1.48/−1.59	*Ec/Hc*	0.98/3.14	0.35/1.13
SD+6H	−3.53	*Hc*	5.90	2.12
SD+3H per period	/	*Hc*	7.41	2.67
SD+1He	−1.33/−1.39	*Ec/Hc*	2.31/3.00	0.83/1.08
SD+1C	−1.79	*Hc*	5.91	2.13
SD+1N	−1.90	*Hc*	5.85	2.10
SD+1O	−1.92	*Hc*	4.32	1.55

Figs. 1 and 2). In the hard core, W atoms form a trigonal prism with H atoms located at the edge of the prism [see Fig. 3(a) and (b)]. Accordingly, five neighboring W atoms are arranged in two shells: the first shell having one H-W bond of 1.94 Å and the second shell having four H-W bonds of 2.04∼2.05 Å, which are slightly longer that in the easy core (1.85∼1.89 Å) but with one more W-H bond.

3.3. Equilibrium concentration of segregated H in SD

Similar to previous studies [23,37], we employ a mean-field model to evaluate the concentration of the segregated H in the SD in W. The equilibrium concentrations of interstitial H in the SD (c_d) and bulk (c_{bulk}) can be estimated as

$$\frac{c_d}{1-c_d} = \frac{c_{bulk}}{1-c_{bulk}} \exp\left(\frac{-E_{seg}(c_d)}{k_B T}\right), \tag{5}$$

where $E_{seg}(c_d)$ is the segregation energy of interstitial H in the SD, which can be expressed as

$$E_{seg}(c_d) = \begin{cases} E^{H-EC}_{seg} \ if \ 0 \le c_d < 0.5 \\ E^{H-EC}_{seg} + 2(c_d - 0.5)\left(E^{H-HC}_{seg} - E^{H-EC}_{seg}\right) \ if \ 0.5 \le c_d \le 1 \end{cases} \tag{6}$$

where E^{H-EC}_{seg} and E^{H-HC}_{seg} are the segregation energy of a single H in the easy core and average segregation energy of H in the hard core (e.g., the case of *SD+3H per period* in Table 1), respectively. Namely, when the concentration of interstitial H in the SD is lower than 0.5, it is assumed that the SD remains the easy-core structure and the interaction of H-H is neglected. Moreover, if the H concentration in the SD reaches up to 1, the whole SD globally transfers into the hard-core structure. Then, the H-dislocation interaction can be described by the average segregation energy of H in the hard-core SD (corresponding to the case of *SD+3H per period* in Table 1). Specifically, when the H concentration in the SD ranges from 0.5 to 1, we employed a linear interpolation to approximate the H segregation energy. Note that this is a rough approximation of H-dislocation interaction, but it will not affect the discussions in the following (since the variation of H segregation energy is less than 0.11 eV).

Also, the interstitial H concentration in the dislocation region and bulk are related to the nominal concentration of H atoms per W, namely, $N_i c_{bulk} + N_d c_d = N_W c_0$, where N_i and N_d are the number of interstitial sites for H occupation in the bulk and dislocation core with volume V, respectively. Apparently, $N_i = 12V/{a_0}^3$ (there are six TISs per W atom and a_0 is the lattice parameter) and $N_d = 3\rho V/b$ (there are three interstitial sites for H per burgers vector and ρ is the dislocation density). N_W is the number of W atoms in the bulk for the same volume, i.e. $N_W = 2V/{a_0}^3$. The above equations can be solved self-consistently to obtain the temperature-dependent concentrations of H in the SD (c_d) as a function of the dislocation density and the nominal H concentration.

Fig. 4 shows the equilibrium concentration of H in the dislocation core as a function of temperature for two different dislocation densities (10^{12} m^{-2} and 10^{14} m^{-2}) and for three different nominal H concentrations (10 appm, 100 appm and 1000 appm). It is clear that the concentration of H in the SD increases with the increasing nominal H concentration and decreases with the increasing dislocation density and temperatures. Importantly, even though the nominal concentration of H is extremely low (∼ 10 appm) and/or the dislocation density is very high (∼ 10^{14} m^{-2}), the equilibrium concentration of H in the dislocation core is still higher than 50% at room temperature due to segregation. These results suggest that the dislocation cores can be easily saturated by interstitial H atoms, leading to the formation of a hard-core configuration.

3.4. Influence of H segregation on SD motion

Naturally, the reconstructed hard core is expected to drastically affect the SD mobility [47,69,70], and likely to pin its motion because the whole “hydride phase” has to move together. To verify this speculation, we determine the critical Peierls stress for the motion of the SD in W with and without H atoms. As shown Fig. 5 and Table 1, the Peierls stress of an isolated SD is 2.78 GPa in pure W without H, consistent with previous studies [47,69]. The introduction of H has a drastic influence on the Peierls stress, which is strongly related to the H-induced reconstruction of core structure and hence H concentration. As shown in Table 1, with a single H, the Peierls stress (∼1.59 GPa) is reduced to about the half of that in pure W (see Table 1), which is consistent with the reduced Peierls energy barrier shown above (see Fig. 2). Also, the reduction of Peierls stress is observed in the cases of two and three H atoms attached to the easy-core structure. However, when more than three H atoms are presented, the easy-to-hard core transition occurs spontaneously. The corresponding Peierls stress reaches 3.14 GPa and 5.90 GPa in the presence of three and six H atoms, respectively, which is much higher than that in pure W. These results suggest that at low H concentrations, one or less H per period, the SD will remain in the easy-core configuration with enhanced mobility, while at higher H concentration, an easy-to-hard core transition occurs for H to suppress the SD mobility. In general, the mobility of hard core is much lower than that of easy core. For example, if one constrained the SD into a local metastable hard-core configuration with two H, the Peierls stress is calculated to be 3.17 GPa, as seen in Table 1, which is much larger than the easy

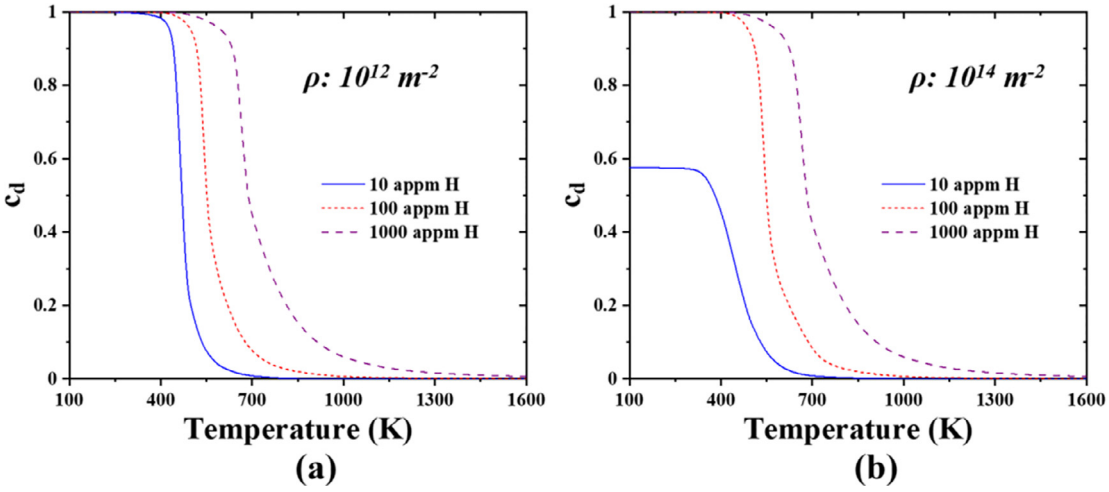

Fig. 4. Temperature dependence of the H concentration segregated in the SD core for three different nominal concentrations of H and two typical density densities, (a) 10^{12} m^{-2} and (b) 10^{14} m^{-2}.

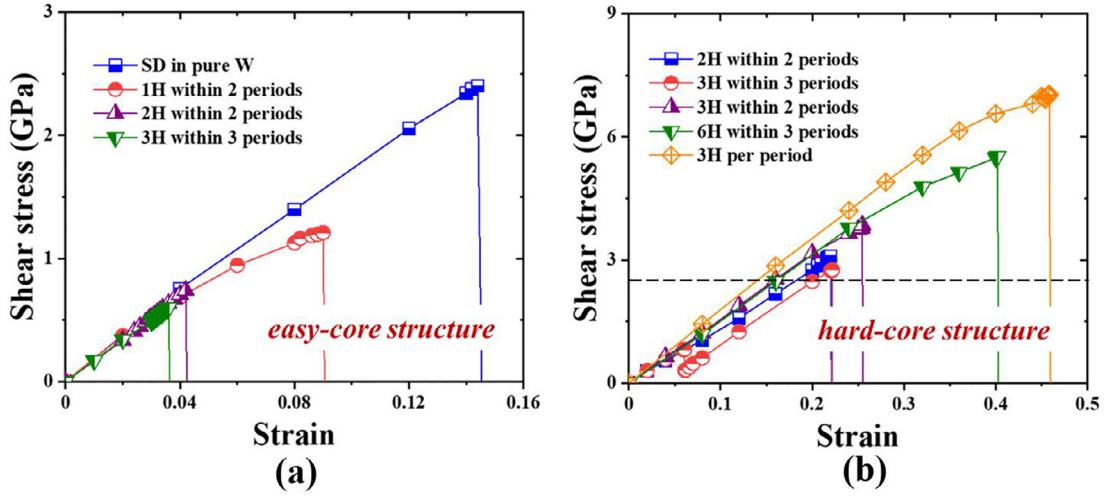

Fig. 5. The DFT calculated shear stress as a function of strain for SD in W with and without H segregation. The dash black line in (b) is the critical shear stress in pure W. Note that the Peierls stress obtained from DFT calculations differs somewhat from that of the isolated dislocation and should be corrected by considering the elastic interaction between dislocations.

core with 2H. With the increasing amount of H segregation, more segments (periods) of SD and then the whole SD will transform into the hard-core structure, to continuously further suppress its mobility. With three H per period, the Peierls stress reaches a very high value of 7.41 GPa (see Table 1).

The above calculations explicitly demonstrated the H-induced easy-to-hard transition of SD core and the corresponding changes of Peierls stresses, which have important implications on the role of H on dislocation mobility. Next, we further illustrate this point by a line-tension model analysis [52,53] to quantitatively estimate the effect of H segregation on SD mobility in W via the kink-pair formation enthalpy (H_{kp}) without external stress. Using our DFT calculated Peierls stresses, segregation energies and known parameters, H_{kp} in pure W is calculated to be ~1.61 eV, which agrees well with previous theories (1.54 eV [60], 1.60 eV [48] and 1.63 eV [71,72]) and experiments (1.75~2.06 eV [54]). The H addition can significantly affect the H_{kp}, which is strongly dependent on the dislocation core structure. As listed in Table S1, when the SD maintains the easy-core structure, the H_{kp} is reduced to 1.20 eV, 1.00 eV and 0.93 eV with the segregation of one, two and three H atoms, respectively, implying the enhancing effect on dislocation motion. However, if the SD transforms into a hard-core and metal hydride-like structure, the corresponding H_{kp} can reach up to 1.65 eV and 2.17 eV in the presence of three and six H atoms (see Table S1), respectively, indicating the suppressing effect on dislocation motion.

It is interesting to note that the H-induced easy-to-hard core transition has also been proposed in bcc Fe from a recent kinetic Monte Carlo simulation, but in that work H segregation was shown to always increase dislocation velocity, despite hard core formation [36]. This difference may be rooted in the different hard-core structure in that the hard core proposed in [36] contains only one H at the center of the trigonal prism, while the hard core we found here contains three H atoms decorating the outside faces of the trigonal prism, like a metal hydride phase.

3.5. Effects of other interstitial solutes on the stability and mobility of SD

Furthermore, we have considered other interstitial solutes, including He, C, N and O, which are known to strengthen the matrix metals even at extremely low concentrations [6,73–76]. Strikingly, their segregation behavior in W is different from H. As listed

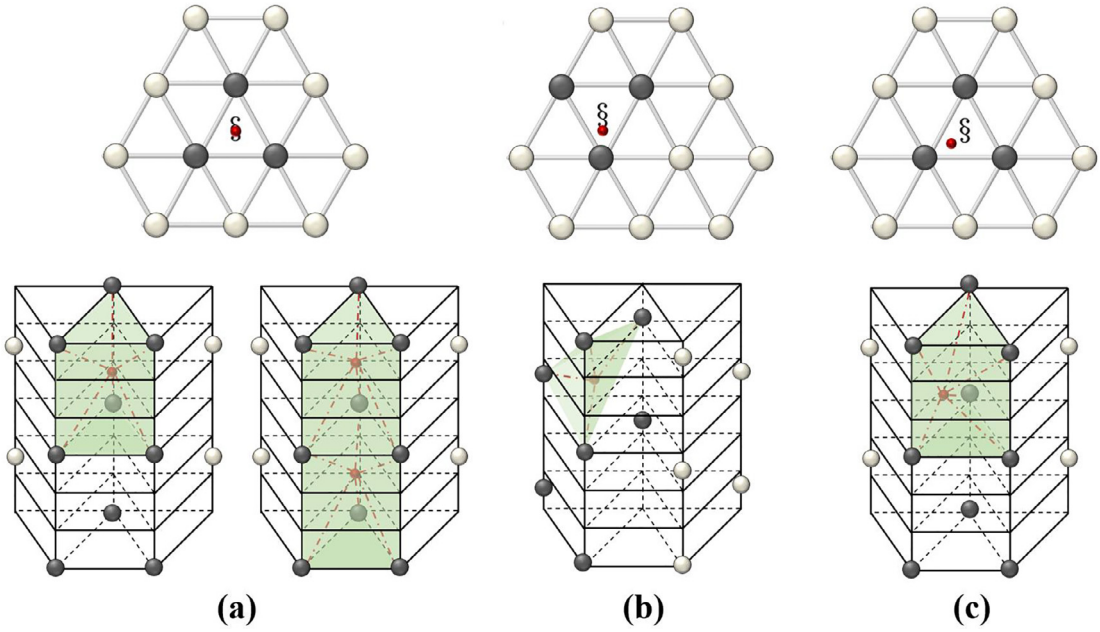

Fig. 6. Local atomic environment of solute (small red spheres) segregation to the SD core in W. The small red spheres denote (a) C/N/O and (b,c) He. Here, two different structures of He segregation are illustrated in (b) and (c) with easy-core (with segregation energy of −1.33 eV) and hard-core (with segregation energy of −1.39 eV) configuration, respectively.

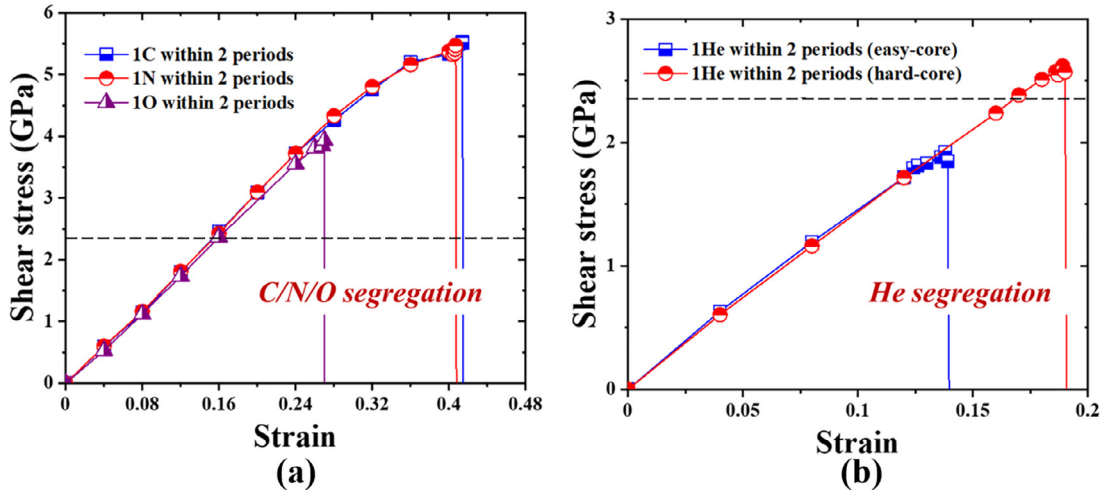

Fig. 7. The DFT calculated shear stress as a function of strain for SD in W with C/N/O/He segregation. For comparison, the critical shear stress in pure W (dash black lines) is also presented. Note that the Peierls stress obtained from DFT calculations differs somewhat from that of the isolated dislocation and should be corrected by considering the elastic interaction between dislocations, as discussed in Section 2.2.

in Table 1, they all tend to segregate to the SD core with a negative segregation energy, which increases with the increasing atomic number, from −1.33/−1.39 eV for He, −1.79 eV for C, −1.90 eV for N to −1.92 eV for O, respectively. Most notably, only one single C/N/O atom segregated into the SD (2*b*) would trigger the local easy-to-hard core transition, similar to recently observed C/N/O/B in Fe [23,77] and C/O in W [78–81]. The segregated C/N/O solute occupies the center of the trigonal prism in the hard core [see Fig. 6(a), left], independent of the initial C/N/O atom position surrounding the dislocation core. Accordingly, the six solute-metal bonds are almost equivalent with a bond length of 2.15∼2.16 Å, 2.13∼2.15 Å and 2.15∼2.18 Å for C, N and O, respectively. When the second C/N/O atom is added, it tends to stay next to the first C/N/O atom along the dislocation line [see Fig. 6(a), right] to minimize the total distortion required for the easy-to-hard transition. As expected, the resulting hard core exhibits very high Peierls stresses, which are 5.91, 5.85 and 4.32 GPa for C, N and O, respectively [see Table 1 and Fig. 7(a)]. Therefore, these solutes will likely always pin the SD motion, as long as they are present in the SD, which is different from prediction by GSFE calculations (see Fig. S1).

As for He segregation to the SD, we found two contrasting scenarios of close segregation energies. If a He atom is placed at the core center initially, the SD remains the easy-core configuration with a segregation energy of −1.33 eV. In this case, similar to H, He is located at a TI-like site in the vicinity of SD and the four shortest He-W bonds are 2 × 1.85 and 2 × 2.20 Å [see Fig. 6(b)], and the Peierls stress is reduced to ∼ 2.31 GPa [see Table 1 and Fig. 7(b)]. However, if He is initially located outside adjacent to the core center, it triggers an easy-to-hard core transition with a segregation energy of −1.39 eV [see Fig. 6(c)], and then the Peierls stress is notably increased to 3.00 GPa [see Table 1 and Fig. 7(b)], to pin the SD motion. Accordingly, six He-W bonds are formed with the

lengths of 2 × 1.84 Å, 2 × 2.35 Å and 2 × 2.56 Å, respectively. Since the energy only differs by less than 5% for the two cases, one expects that He will likely pin the SD motion, showing a very weak or no concentration dependence.

It is important to note that the largest supercell employed in present work only contains 3 units of repetition (i.e. 3 × ***b***) along the dislocation line. Thus, there is a concern that if the length of dislocation line becomes longer, the easy-to-hard core transition may not occur upon segregation of a single He/C/N/O into SD in W. However, previous DFT studies [79,81] showed that the opposite is true. The local reconstructions of dislocation cores remain to be present in larger supercells (up to 10 × ***b*** in [81] and 8 × ***b*** in [79]) upon the segregation of one solute atom. For example, Bakaev et al. [79] investigated the interaction of a single C with SD in W using large simulation boxes with the dislocation length up to 8 × ***b***. It is found that the dislocation core has a hard-core structure next to the C atom, while at the distance of 4 × ***b*** the core structure reverts back to the easy-core configuration. Therefore, even in an "infinitely" long dislocation line, the segregation of a single He/C/N/O atom can still locally, albeit not completely, convert the core structure into the hard-core configuration.

Similarly, based on the line-tension model, calculated Peierls stresses and segregation energy, we further calculate the H_{kp} of SD in W with the segregation of C/N/O/He. As expected, the H_{kp} is increased to 2.21 eV, 2.19 eV and 1.88 eV for C, N and O segregation, respectively (see Table S1), which is much higher than that of pure W (∼ 1.61 eV). For the segregation of a He atom, the corresponding H_{kp} is also related to the dislocation core structure, in which the H_{kp} of easy-core structure is much lower than that of hard-core structure (see Table S1).

4. Conclusions

We discover theoretically an interesting effect of easy-to-hard core transition of SD induced by H segregation in bcc W, based on first-principles calculations. Such H-induced core reconstruction is concentration-dependent, i.e., occurring only above a critical concentration. Before transition, owing to multiple local energy-minimum positions for H in the easy core, the H atoms are attached to the "periphery" of dislocation and effectively reduce Peierls barrier/stress and hence kink-pair formation enthalpy, tending to enhance the dislocation mobility by moving along with SD in a concerted fashion. In contrast, after transition, the hard-core adopt a metal hydride-like phase, as H atoms become the "body" of dislocation to significant increase the Peierls stress and kink-pair formation enthalpy, tending to pin dislocation motion in W. Differently, the segregation of just one solute of other elements, such as He, C, N and O, in a three-period core (i.e. 3 × ***b***) will induce the local SD hard-core formation and appear to always pin the SD motion. Our findings advocate that the solute-induced structural transition of dislocation core can be a common mechanism to drastically modify many dislocation properties, notably shedding new light on understanding the effect of solute on dislocation mobility. Such transition may even occur at very low solute concentration independent of metal-solute bond strength, and thus should be accounted for in many phenomena related to solute-defect interactions.

Declaration of Competing Interest

The authors declare that they have no known competing financial interests or personal relationships that could have appeared to influence the work reported in this paper.

Acknowledgments

This research is financially supported by the National Natural Science Foundation of China with Grant Nos. 11905135 and 12075022, and the Major Program of National Natural Science Foundation of China with Grant No. 12192281. F.L. thanks support from U.S. DOE-BES (Grant No. DE- FG02-04ER46148).

Supplementary materials

Supplementary material associated with this article can be found, in the online version, at doi:10.1016/j.actamat.2022.117622.

References

[1] Z. Wu, W.A. Curtin, The origins of high hardening and low ductility in magnesium, Nature 526 (2015) 62–67.
[2] L. Dezerald, D. Rodney, E. Clouet, L. Ventelon, F. Willaime, Plastic anisotropy and dislocation trajectory in BCC metals, Nat. Commun. 7 (2016) 11695.
[3] D. Rodney, L. Ventelon, E. Clouet, L. Pizzagalli, F. Willaime, Ab initio modeling of dislocation core properties in metals and semiconductors, Acta Mater. 124 (2017) 633–659.
[4] L. Proville, D. Rodney, M.C. Marinica, Quantum effect on thermally activated glide of dislocations, Nat. Mater. 11 (2012) 845–849.
[5] D.R. Trinkle, C. Woodward, The chemistry of deformation: how solutes soften pure metals, Science 310 (2005) 1665–1667.
[6] Q. Yu, L. Qi, T. Tsuru, R. Traylor, D. Rugg, J.W. Morris, M. Asta, D.C. Chrzan, A.M. Minor, Origin of dramatic oxygen solute strengthening effect in titanium, Science 347 (2015) 635–639.
[7] G.P. Leyson, W.A. Curtin, L.G. Hector, C.F. Woodward, Quantitative prediction of solute strengthening in aluminium alloys, Nat. Mater. 9 (2010) 750–755.
[8] W.H. Johnson, Proceedings of the royal society of londonengineering fracture mechanics, Proc. R. Soc. Lond. 23 (1874) 168–179.
[9] J.M. Cairney, Atoms on the move-finding the hydrogen, Science 355 (2017) 1128–1129.
[10] I.M. Robertson, P. Sofronis, A. Nagao, M.L. Martin, S. Wang, D.W. Gross, K.E. Nygren, Hydrogen embrittlement understood, Metall. Mater. Trans. A 46 (2015) 2323–2341.
[11] S.P. Lynch, in: Stress Corrosion Cracking-II Hydrogen Embrittlement (HE) Phenomena and Mechanisms, Woodhead Publishing, 2011, p. 90.
[12] H.K. Birnbaum, P. Sofronis, Hydrogen-enhanced localized plasticity-a mechanism for hydrogen-related fracture, Mater. Sci. Eng. A 176 (1994) 191–202.
[13] S. Yin, G. Cheng, T.H. Chang, G. Richter, Y. Zhu, H. Gao, Hydrogen embrittlement in metallic nanowires, Nat. Commun. 10 (2019) 2004.
[14] Y. Murakami, T. Kanezaki, Y. Mine, Hydrogen effect against hydrogen embrittlement, Metall. Mater. Trans. A 41 (2010) 2548–2562.
[15] M.L. Martin, J.A. Fenske, G.S. Liu, P. Sofronis, I.M. Robertson, On the formation and nature of quasi-cleavage fracture surfaces in hydrogen embrittled steels, Acta Mater. 59 (2011) 1601–1606.
[16] M. Seita, J.P. Hanson, S. Gradecak, M.J. Demkowicz, The dual role of coherent twin boundaries in hydrogen embrittlement, Nat. Commun. 6 (2015) 6164.
[17] J. Song, W.A. Curtin, Atomic mechanism and prediction of hydrogen embrittlement in iron, Nat. Mater. 12 (2013) 145–151.
[18] M.L. Martin, M. Dadfarnia, A. Nagao, S. Wang, P. Sofronis, Enumeration of the hydrogen-enhanced localized plasticity mechanism for hydrogen embrittlement in structural materials, Acta Mater. 165 (2019) 734–750.
[19] J.P. Chateau, D. Delafosse, T. Magnin, Numerical simulations of hydrogen–dislocation interactions in fcc stainless steels.: part I: hydrogen–dislocation interactions in bulk crystals, Acta Mater. 50 (2002) 1507–1522.
[20] D. Xie, S. Li, M. Li, Z. Wang, P. Gumbsch, J. Sun, E. Ma, J. Li, Z. Shan, Hydrogenated vacancies lock dislocations in aluminium, Nat. Commun. 7 (2016) 13341.
[21] T. Kaplan, F. Liu, M. Mostoller, M.F. Chisholm, V. Milman, First-principles study of impurity segregation in edge dislocations in Si, Phys. Rev. B 61 (2000) 1674–1676.
[22] A. Bakaev, P. Grigorev, D. Terentyev, A. Bakaeva, E.E. Zhurkin, Y.A. Mastrikov, Trapping of hydrogen and helium at dislocations in tungsten: an ab initio study, Nucl. Fusion 57 (2017) 126040.
[23] L. Ventelon, B. Lüthi, E. Clouet, L. Proville, B. Legrand, D. Rodney, F. Willaime, Dislocation core reconstruction induced by carbon segregation in bcc iron, Phys. Rev. B 91 (2015) 220102(R).
[24] Y.S. Chen, H. Lu, J. Liang, A. Rosenthal, H. Liu, G. Sneddon, I. McCarroll, Z. Zhao, W. Li, A. Guo, J.M. Cairney, Observation of hydrogen trapping at dislocations, grain boundaries, and precipitates, Science 367 (2020) 171–175.
[25] H.A. Cottrell, B.A. Bilby, in: Dislocation theory of yielding and strain ageing of iron, 62, 1949, pp. 49–62.
[26] J. Song, W.A. Curtin, Mechanisms of hydrogen-enhanced localized plasticity: an atomistic study using α-Fe as a model system, Acta Mater. 68 (2014) 61–69.
[27] P. Grigorev, T.D. Swinburne, J.R. Kermode, Hybrid quantum/classical study of hydrogen-decorated screw dislocations in tungsten: ultrafast pipe diffusion, core reconstruction, and effects on glide mechanism, Phys. Rev. Mater. 4 (2020) 023601.

[28] H. Matsui, H. Kimura, A. Kimura, The effect of hydrogen on the mechanical properties of high purity iron III. The dependence of softening in specimen size and charging current density, Mater. Sci. Eng. 40 (1979) 227–234.
[29] H. Matsui, H. Kimura, S. Moriya, The effect of hydrogen on the mechanical properties of high purity iron I. Softening and hardening of high purity iron by hydrogen charging during tensile deformation, Mater. Sci. Eng. 40 (1979) 207–216.
[30] T. Tabata, H. Birnbaum, Direct observations of the effect of hydrogen on the behavior of dislocations in iron, Scr. Metall. 17 (1983) 947–950.
[31] M. Koyama, S.M. Taheri-Mousavi, H. Yan, J. Kim, B.C. Cameron, S.S. Moeini-Ardakani, J. Li, C.C. Tasan, Origin of micrometer-scale dislocation motion during hydrogen desorption, Sci. Adv. 6 (2020) eaaz1187.
[32] Y. Zhao, G. Lu, QM/MM study of dislocation-hydrogen/helium interactions in α-Fe, Model. Simul. Mater. Sci. Eng. 19 (2011) 065004.
[33] I. Robertson, The effect of hydrogen on dislocation dynamics, Eng. Fract. Mech. 68 (2001) 671–692.
[34] M. Itakura, H. Kaburaki, M. Yamaguchi, T. Okita, The effect of hydrogen atoms on the screw dislocation mobility in bcc iron: a first-principles study, Acta Mater. 61 (2013) 6857–6867.
[35] I.H. Katzarov, D.L. Pashov, A.T. Paxton, Hydrogen embrittlement I. Analysis of hydrogen-enhanced localized plasticity: effect of hydrogen on the velocity of screw dislocations in α-Fe, Phys. Rev. Mater. 1 (2017) 033602.
[36] P. Gong, I.H. Katzarov, J. Nutter, A.T. Paxton, W.M. Rainforth, The influence of hydrogen on plasticity in pure iron-theory and experiment, Sci. Rep. 10 (2020) 10209.
[37] Y. Wang, X. Wang, X. Wu, Q. Li, C. Li, G. Shu, B. Xu, W. Liu, Hydrogen distribution induced screw dislocation core spreading in tungsten, J. Nucl. Mater. 523 (2019) 71–79.
[38] G. Kresse, J. Hafner, Ab initio molecular dynamics for liquid metals, Phys. Rev. B 47 (1993) 558–561.
[39] G. Kresse, J. Furthmüller, Efficient iterative schemes for ab initio total-energy calculations using a plane-wave basis set, Phys. Rev. B 54 (1996) 11169.
[40] P.E. Blöchl, Projector augmented-wave method, Phys. Rev. B 50 (1994) 17953–17979.
[41] J.P. Perdew, K. Burke, M. Ernzerhof, Generalized gradient approximation made simple, Phys. Rev. Lett. 77 (1996) 3865–3868.
[42] H.J. Monkhorst, J.D. Pack, Special points for Brillouin-zone integrations, Phys. Rev. B 13 (1976) 5188–5192.
[43] L. Ventelon, F. Willaime, Core structure and Peierls potential of screw dislocations in α-Fe from first principles: cluster versus dipole approaches, J. Comput. Aided Mater. 14 (2007) 85–94.
[44] E. Clouet, L. Ventelon, F. Willaime, Dislocation core energies and core fields from first principles, Phys. Rev. Lett. 102 (2009) 055502.
[45] G. Henkelman, B.P. Uberuaga, H. Jonsson, A climbing image nudged elastic band method for finding saddle points and minimum energy path, J. Chem. Phys. 113 (2000) 9901–9904.
[46] G. Henkelman, H. Jonsson, Improved tangent estimate in the nudged elastic band method for finding minimum energy paths and saddle points, J. Chem. Phys. 113 (2000) 9978–9985.
[47] L. Romaner, C. Ambrosch-Draxl, R. Pippan, Effect of rhenium on the dislocation core structure in tungsten, Phys. Rev. Lett. 104 (2010) 195503.
[48] H. Li, C. Draxl, S. Wurster, R. Pippan, L. Romaner, Impact of d-band filling on the dislocation properties of bcc transition metals: the case of tantalum-tungsten alloys investigated by density-functional theory, Phys. Rev. B 95 (2017) 094114.
[49] W. Cai, V.V. Bulatov, J. Chang, J. Li, S. Yip, Anisotropic elastic interactions of a periodic dislocation array, Phys. Rev. Lett. 86 (2001) 5727–5730.
[50] W. Cai, V.V. Bulatob, J. Chang, J. Li, S. Yip, Periodic image effects in dislocation modelling, Philos. Mag. 83 (2003) 539–567.
[51] R.A. Ayres, G.W. Shannette, D.F. Stein, Elastic constants of tungsten−rhenium alloys from 77 to 298K, J. Appl. Phys. 46 (1975) 1526–1530.
[52] J.E. Dorn, S. Rajnak, Nucleation of kink pairs and the Peierls' mechanism of plastic deformation, Trans. Metall. Soc. AIME 230 (1964) 1052–1064.
[53] P. Guyot, J.E. Dorn, A critical review of the Peierls mechanism, Can. J. Phys. 45 (1967) 983–1016.
[54] D. Brunner, Comparison of flow-stress measurements on high-purity tungsten single crystal with the kink-pair theory, Mater. Trans. JIM 41 (2000) 152–160.
[55] C.R. Weinberger, G.J. Tucker, S.M. Foiles, Peierls potential of screw dislocations in bcc transition metals: predictions from density functional theory, Phys. Rev. B 87 (2013) 054114.
[56] N. Fernandez, Y. Ferro, D. Kato, Hydrogen diffusion and vacancies formation in tungsten: density functional theory calculations and statistical models, Acta Mater. 94 (2015) 307–318.
[57] Y.J. Hu, M.R. Fellinger, B.G. Butler, Y. Wang, K.A. Darling, L.J. Kecskes, D.R. Trinkle, Z.K. Liu, Solute-induced solid-solution softening and hardening in bcc tungsten, Acta Mater. 141 (2017) 304–316.
[58] L. Hu, H. Huang, Z. Wang, W. Jiang, X. Ni, Y. Zhou, V. Zielasek, M.G. Lagally, B. Huang, F. Liu, Ubiquitous spin-orbit coupling in a screw dislocation with high spin coherency, Phys. Rev. Lett. 121 (2018) 066401.
[59] H.B. Zhou, S. Jin, Y. Zhang, G.H. Lu, F. Liu, Anisotropic strain enhanced hydrogen solubility in bcc metals: the independence on the sign of strain, Phys. Rev. Lett. 109 (2012) 135502.
[60] L. Dezerald, L. Proville, L. Ventelon, F. Willaime, D. Rodney, First-principles prediction of kink-pair activation enthalpy on screw dislocations in bcc transition metals: V, Nb, Ta, Mo, W, and Fe, Phys. Rev. B 91 (2015) 094105.
[61] G.P.M. Leyson, B. Grabowski, J. Neugebauer, Multiscale description of dislocation induced nano-hydrides, Acta Mater. 89 (2015) 50–59.
[62] J. Hou, X.S. Kong, X. Wu, J. Song, C.S. Liu, Predictive model of hydrogen trapping and bubbling in nanovoids in bcc metals, Nat. Mater. 18 (2019) 833–839.
[63] D. Terentyev, V. Dubinko, A. Bakaev, Y. Zayachuk, W. Van Renterghem, P. Grigorev, Dislocations mediate hydrogen retention in tungsten, Nucl. Fusion 54 (2014) 042004.
[64] Z.A. Piazza, M. Ajmalghan, Y. Ferro, R.D. Kolasinski, Saturation of tungsten surfaces with hydrogen: a density functional theory study complemented by low energy ion scattering and direct recoil spectroscopy data, Acta Mater. 145 (2018) 388–398.
[65] H.B. Zhou, Y.L. Liu, S. Jin, Y. Zhang, G.N. Luo, G.H. Lu, Investigating behaviours of hydrogen in a tungsten grain boundary by first principles: from dissolution and diffusion to a trapping mechanism, Nucl. Fusion 50 (2010) 025016.
[66] R. Kirchheim, Reducing grain boundary, dislocation line and vacancy formation energies by solute segregation. I. Theoretical background, Acta Mater. 55 (2007) 5129–5138.
[67] R. Kirchheim, Revisiting hydrogen embrittlement models and hydrogen-induced homogeneous nucleation of dislocations, Scr. Mater. 62 (2010) 67–70.
[68] R. Kirchheim, Solid solution softening and hardening by mobile solute atoms with special focus on hydrogen, Scr. Mater. 67 (2012) 767–770.
[69] Y.H. Li, H.B. Zhou, L. Liang, N. Gao, H. Deng, F. Gao, G. Lu, G.H. Lu, Transition from ductilizing to hardening in tungsten: the dependence on rhenium distribution, Acta Mater. 181 (2019) 110–123.
[70] R. Gröger, A.G. Bailey, V. Vitek, Multiscale modeling of plastic deformation of molybdenum and tungsten: I. Atomistic studies of the core structure and glide of 1/2<111>screw dislocations at 0 K, Acta Mater. 56 (2008) 5401–5411.
[71] A. Stukowski, D. Cereceda, T.D. Swinburne, J. Marian, Thermally-activated non-schmid glide of screw dislocations in W using atomistically-informed kinetic Monte Carlo simulations, Int. J. Plast. 65 (2015) 108–130.
[72] D. Cereceda, M. Diehl, F. Roters, D. Raabe, J.M. Perlado, J. Marian, Unraveling the temperature dependence of the yield strength in single-crystal tungsten using atomistically-informed crystal plasticity calculations, Int. J. Plast. 78 (2016) 242–265.
[73] A.R. Troiano, The role of hydrogen and other interstitials in the mechanical behavior of metals, Metallogr. Microstruct. Anal. 5 (2016) 557–569.
[74] D. Caillard, J. Bonneville, Dynamic strain aging caused by a new Peierls mechanism at high-temperature in iron, Scr. Mater 95 (2015) 15–18.
[75] P.J. Yang, Q.J. Li, T. Tsuru, S. Ogata, J.W. Zhang, H.W. Sheng, Z.W. Shan, G. Sha, W.Z. Han, J. Li, E. Ma, Mechanism of hardening and damage initiation in oxygen embrittlement of body-centred-cubic niobium, Acta Mater. 168 (2019) 331–342.
[76] M.G. Jo, P.P. Madakashira, J.Y. Suh, H.N. Han, Effect of oxygen and nitrogen on microstructure and mechanical properties of vanadium, Mater. Sci. Eng. A 675 (2016) 92–98.
[77] B. Lüthi, L. Ventelon, D. Rodney, F. Willaime, Attractive interaction between interstitial solutes and screw dislocations in bcc iron from first principles, Comput. Mater. Sci. 148 (2018) 21–26.
[78] B. Lüthi, L. Ventelon, C. Elsässer, D. Rodney, F. Willaime, First principles investigation of carbon-screw dislocation interactions in body-centered cubic metals, Model. Simul. Mater. Sci. Eng. 25 (2017) 084001.
[79] A. Bakaev, A. Zinovev, D. Terentyev, G. Bonny, C. Yin, N. Castin, Y.A. Mastrikov, E.E. Zhurkin, Interaction of carbon with microstructural defects in a W-Re matrix: an ab initio assessment, J. Appl. Phys. 126 (2019) 075110.
[80] Y. Zhao, L. Dezerald, J. Marian, Electronic structure calculations of oxygen atom transport energetics in the presence of screw dislocations in tungsten, Metals 9 (2019) 252.
[81] G. Hachet, L. Ventelon, F. Willaime, E. Clouet, Screw dislocation-carbon interaction in BCC tungsten: an ab initio study, Acta Mater. 200 (2020) 481–489.